

Live-Cell Imaging of Vesicle Trafficking and Divalent Metal Ions by Total Internal Reflection Fluorescence (TIRF) Microscopy

Merewyn K. Loder, Takashi Tsuboi, and Guy A. Rutter

Abstract

Total internal reflection fluorescence (TIRF) microscopy is an especially powerful tool for visualizing live cellular events. Fluorescent molecules alone provide broad information about the expression and localization of proteins and other molecules; however, the temporal and spatial resolution is confounded by signal from outside the area of interest and the intensity of the illumination required. TIRF overcomes this limitation by using the reflective properties of a laser beam to illuminate a narrow (<100 nm) strip at the surface of a cell with a relatively low powered evanescent wave, thus making it possible to measure events occurring specifically at the plasma membrane such as exocytosis, single molecule interactions, and ionic changes during signal transduction. Here we describe some of the methods for using TIRF microscopy to study the processes involved in exocytosis from excitable cells (i.e., neurons, endocrine, neuroendocrine, and exocrine cells) and the release of physiologically active substances (i.e., neurotransmitters, hormones, and mucus).

The failure of regulated exocytosis is associated with various diseases such as allergy, brain dysfunction, and endocrine illness. Diabetes mellitus, which is due to an absolute (type I) or relative (type II) deficiency of insulin secretion from pancreatic β -cells, is a major area of therapeutic interest. Insulin is stored in dense core vesicles with Zn^{2+} ions in pancreatic β -cells. Insulin secretion is regulated by plasma glucose concentration which acts through intracellular metabolism to influence intracellular $[\text{Ca}^{2+}]$. However, the precise molecular mechanisms controlling insulin granule movement towards, and fusion at, the plasma membrane remain only partially understood. To tackle this problem, we have used live cell imaging techniques to image regulated exocytosis in single living β -cells alongside intracellular Ca^{2+} and Zn^{2+} concentrations.

Key words: Exocytosis, Insulin, Calcium, Zinc, Pancreatic β -cells, Total internal reflection fluorescence microscopy

1. Introduction

Optical live cell imaging techniques represent a powerful tool for detecting molecular events such as cell adhesion, secretion of hormones, and intracellular signal transduction in live cells.

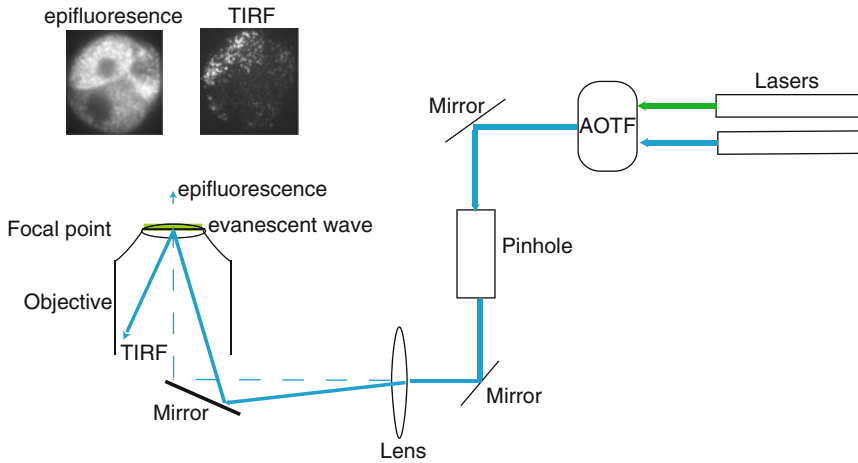


Fig. 1. Schematic of a typical TIRF microscope (system 2) and representative images of a cluster of three β -cells under epifluorescent (*left*) and TIRF (*right*) illumination.

Epifluorescence imaging of live cells can provide information on the dynamics of protein localization and molecular interactions, as well as the intracellular concentrations of signal transduction molecules and ions. However, at high objective magnification under epifluorescence, there is poor vertical spatial resolution and fluorescence from outside the focal plane can overwhelm the images limiting the use of this technique for studying active cellular processes (Fig. 1). To overcome this limitation, total internal reflection fluorescence (TIRF) microscopy was developed by Daniel Axelrod in the early 1980s (1, 2).

TIRF microscopy employs an angled excitation laser light and excites fluorophores just beneath a glass-water interface with extremely high vertical spatial resolution. A laser beam, hitting a substance of different refractive index to the one in which it is travelling, bends. In TIRF microscopy, the laser irradiates the specimen at an angle of incidence greater than or equal to the critical angle of refraction whereby the excitation laser light is totally reflected. The reflection generates a very thin electromagnetic field (~ 200 nm) in the specimen. This field, called the evanescent wave or field, undergoes exponential intensity decay with increasing distance from the surface. Thus, only those fluorophores within 200 nm of the specimen interface are excited, providing high vertical spatial resolution fluorescence images suitable for studying rapid active biological events. Release of hormones via regulated exocytosis in response to a physiological stimulus is a fast, dynamic and complex process requiring the trafficking of cargo to the plasma membrane, reorganization of the cytoskeleton and actin networks (3–5), and the fusion of vesicles with the plasma membrane through protein recruitment to the soluble NSF attachment protein

receptors (SNARE) complex (6). Many diseases, from depression to diabetes, involve perturbations of these processes. Thus, understanding of the behavior of secretory granules at the plasma membrane and of the regulatory molecules involved is an essential goal of modern cell biology.

With high speed data acquisition and ultra sensitive charge-coupled device (CCD) cameras, TIRF microscopy has been used to observe the exocytotic release of glutamate in astrocytes (7), to measure changes in Ca^{2+} concentration beneath the plasma membrane (8), and to investigate dense-core vesicle behavior (4, 9–13). We have employed TIRF to visualize insulin exocytosis and intracellular Ca^{2+} and Zn^{2+} signaling in pancreatic β -cells and here we describe the details of this technique.

2. Materials

2.1. Equipment

There are many types of TIRF configurations including the use of either a prism or illumination “through the lens”; the latter is the most common in molecular biology and requires a ultra high numerical aperture (NA) objective. Here, we describe two configurations used in our laboratories: System 1 a Nikon TIRF microscope and System 2 based on a Zeiss Axiovert microscope. System 1 was largely used to generate the granule movement data described whereas system 2 was used for the plasma membrane divalent cations studies. However, the methods described can be used interchangeably.

2.1.1. System 1: Nikon TIRF Microscope

1. An ultra high numerical aperture (NA) objective lens (CFI Apo TIRF 100 \times H, NA=1.49; Nikon) is mounted on a nosepiece of a Ti-E inverted microscope. Immersion oil (Cargille Laboratories) of a high refractive index ($n=1.515$) is used to couple the lens to the glass dish. Excitation laser light from a diode pumped solid-state (DPSS) laser (wave length=488 nm, 30 mW; Spectra Physics) is introduced to an optical fiber. The light from the optical fiber is focused with two illumination lenses on the back focal plane near the extreme edge of the objective lens. By theoretical calculation, the space constant for exponential decay of the evanescent field was estimated to be 100 nm (see Note 1).
2. To excite the green fluorescent protein (GFP), or the yellow fluorescent protein (YFP) variant Venus, we use a 488 nm DPSS laser. For imaging of green fluorescence, we use a dichroic mirror (T510LPXRXT, Chroma) which divides the blue and green components of the images. We then use a 515–550 nm band-pass filter (ET535/50m, Chroma) to obtain the green fluorescence

component. A computer-controlled electromagnetically driven shutter (VMM-D3J, Uniblitz) is placed between the optical fiber and illumination lenses to prevent photobleaching of the cells between image acquisitions. The shutter is opened synchronously with an electron multiply charge-coupled device (EM-CCD) camera (DU897E-CS0-#BV, Andor Technology) and exposure controlled with MetaMorph software (version 7.7, Molecular Devices).

2.1.2. System 2: Zeiss Axiovert TIRF Microscope

1. An ultra high numerical aperture objective lens (Apo 100× H, NA = 1.45) is mounted on the nosepiece of an Axiovert 200M inverted microscope. Immersion oil (Olympus) of a high refractive index ($n = 1.517$) is used to couple the lens to a glass coverslip. Cells are excited using a DPSS laser (473 nm, 80 mW; Crystalaser). Emitted light is separated using a double dichroic (590/22bs), magnified with an 1.6× optovar. For two color imaging, the emitted light is split into two channels using a Dualview (Optical Insights) image splitter with a dichroic cut-off at 585 nm (T585LP) and band-pass filters 595–670 nm (ET630-75) and 485–550 nm (ET517/65M) (all filters from Chroma). Separate images of the two channels are taken on an iXonEM+ EM-CCD camera (Andor Scientific) controlled by Andor IQ software. Images shown are acquired at 20 Hz and 50 ms exposure at 100 nm/pixel. The light from the lasers is focused through a pinhole via two illumination lenses on to the back focal plane near the extreme edge of the objective lens. By theoretical calculation, the space constant for exponential decay of the evanescent field is estimated to be 100 nm (see Note 1).
2. For high resolution granule movement studies using system 2, we use a higher numerical aperture lens (1.65 NA 100× ApoTIRF, Olympus), special immersion oil with a very high refractive index ($n = 1.78$ SPI supplies), and TIRF coverslips (035055-9-U990, Olympus).

2.2. Cell Preparation (See Note 2)

2.2.1. MIN6 Cells

1. Dulbecco's modified Eagle's medium (DMEM, high glucose) supplemented with 10% fetal bovine serum (FBS), 100 U/mL penicillin, 100 µg/mL streptomycin, and 30 µM 2-mercaptoethanol.
2. Phosphate-buffered saline (PBS): pH 7.4, without CaCl_2 and MgCl_2 .
3. Trypsin 0.25% with 1 mM ethylenediaminetetraacetic acid (EDTA) solution.
4. Poly-L-lysine (PLL): 1 mg/mL.
5. Glass-bottom 35-mm dishes treated with PLL in PBS for 30 min.

6. MIN6 cells (passage # 19–30; a gift from Prof. Junichi Miyazaki, Osaka University, Osaka, Japan) (14).
7. Lipofectamine 2000 (Invitrogen)

2.2.2. Primary Pancreatic β -Cells

1. Female CD1 mice age 12–16 weeks.
2. RPMI 1640 medium: 10 mM glucose and 2 mM glutamine supplemented with 10% FBS, 100 U/mL penicillin, and 100 μ g/mL streptomycin.
3. Ca^{2+} -free buffer: 138 mM NaCl, 5.6 mM KCl, 1.2 mM MgCl_2 , 5 mM HEPES, 1 mM EDTA, 100 U/mL penicillin, and 100 μ g/mL streptomycin, pH 7.35. Alternatively: 0.05% Trypsin/0.02% EDTA.
4. Type IV collagenase.
5. Poly-L-lysine (PLL): 1 mg/mL.
6. Glass-bottom 35-mm dishes or 22 mm coverslips treated with PLL in PBS for 30 min.

2.3. Probes Used for the Labeling of Dense Core Vesicles

2.3.1. Neuropeptide Y Plasmid Used for Labeling MIN6 Cells

Human preproneuropeptide Y (NPY) cDNA lacking a TGA stop codon was amplified by PCR using a forward primer, 5'-GAATTCATGCTAGGTAACAAGCGACT-3' (primer #1; *Eco*RI site underlined), and reverse primer, 5'-GGATCCCAATTGCAGGGTCTTCA-3' (primer #2; *Bam*HI site underlined), where TGA is replaced by TGG. The PCR product was subcloned into a pCR2.1 vector (Invitrogen). The NPY cDNA fragment lacking a stop codon was cleaved with *Eco*RI/*Bam*HI and subcloned into the *Eco*RI/*Bam*HI site of the multiple cloning site of a yellow fluorescent protein variant expression vector (pVenus-N1) (15).

2.3.2. Adenoviral Probe Used for Labeling Primary Cultured β -Cells

Recombinant adenovirus encoding NPY-Venus (NPY-Venus) was prepared using the AdEasy system (16, 17). A DNA fragment encoding fused NPY and Venus cDNAs was generated using PCR with the NPY-Venus plasmid as template. The forward primer, 5'-GTCGACGACGAGATGCTAGGTAACAAGCGA included a *Sa*II restriction site (underlined) and Kozak sequence (italicized), and the reverse primer, 5'-TGCGGCCGCTTACTTGTACAGCTC, contained the Venus stop codon and a *Not*I restriction site (underlined). The *Sa*II–*Not*I fragment, comprising full-length NPY-Venus, was purified and ligated into plasmid pShuttle-CMV under the control of the human cytomegalovirus promoter. Co-transformation of competent RecA⁺ bacteria (XL1-B) with the above construct and the adenoviral pAdEasy-1 vector generated recombinant adenoviral plasmid, which was purified and transfected into HEK293 cells. The transfected cells were readily monitored through Venus fluorescence, and adenoviral particles obtained by the extraction from the cells 10 days after transfection. The virus was further amplified and purified by centrifugation on a CsCl gradient. Stocks

of 10^9 – 10^{10} infectious particles per milliliter were retained and used in experiments. Titration of the virus was performed by infecting HEK293 cells with serially diluted viral stocks, and counting positive cells through Venus fluorescence (18).

2.4. Reagents for TIRF Imaging

1. Krebs-Ringer bicarbonate (KRB) solution: 125 mM NaCl, 3.5 mM KCl, 1.5 mM CaCl_2 , 0.5 mM MgSO_4 , 0.5 mM KH_2PO_4 , 25 mM NaHCO_3 , 3 mM glucose, and 10 mM HEPES; pH 7.4 equilibrated with 95:5 O_2/CO_2 .
2. High glucose-containing KRB: KRB with 25 mM glucose.
3. High-KCl-containing KRB: Stimulation with KCl is achieved by perfusion of 50 mM KCl-containing KRB (NaCl is reduced to maintain the osmolarity).
4. Trypsin 0.25% with 1 mM ethylenediaminetetraacetic acid (EDTA) solution
5. Poly-L-lysine (PLL): 1 mg/mL
6. Glass coverslips and 6-well plates
7. RPMI medium, supplemented with 10% FBS and 3 mM glucose
8. 2 μM Fura Red-AM: 2 mM stock solution Fura Red-AM in DMSO, diluted in KRB solution, and sonicated for 10 s to ensure resuspension.
9. 3 μM FluoZin-3 AM

3. Methods

3.1. Cleaning and Coating of Glass-Bottom 35-mm Dishes

1. Clean glass-bottom 35-mm dishes by first placing them into a 500 mL beaker containing 300 mL of Milli-Q water, and then place the beaker in an ultrasound bath for 1 h.
2. Dip the glass-bottom 35-mm dishes into another 500 mL beaker containing 300 mL of 70% ethanol for 1 h (see Note 3).
3. Take out glass-bottom 35-mm dishes from the beaker inside a cell culture clean bench, then sterilize them using a UV lamp for 30 min in the clean bench.
4. Apply 100 μL of PLL solution onto each glass-bottom 35-mm dish.
5. After 30 min, remove the PLL solution and wash three times with 1 mL of sterile PBS.

3.2. Transfection of Dense Core Vesicle Marker to MIN6 Cells

1. Culture cells in a 10-cm Petri dish and incubate in 5% CO_2 at 37°C .
2. For TIRF imaging, plate the cells in PLL-coated glass-bottom 35-mm dishes.

3. Transfect the MIN6 cells with 3 μg of NPY–Venus vector using Lipofectamine 2000 according to the manufacturer’s instructions. All TIRF experiments are performed 2 days after transfection.

3.3. Adenoviral Infection to Primary Pancreatic β -Cells

1. *Preparation of mouse β -cells:* For preparation of mouse islets of Langerhans, a detailed isolation procedure by collagenase digestion is described by Ravier and Rutter (19). Briefly, islets are isolated by collagenase digestion of the pancreas of female CD1 mice and selected by hand-picking or histopaque gradient centrifugation. Islets are then cultured in RPMI 1640 for 1 day. Islets are dissociated after incubation in Ca^{2+} -free buffer or Trypsin EDTA for 5 min. After brief centrifugation, the solution is replaced with RPMI 1640, and the islets disrupted by pipetting through a glass pipette. After this procedure, the disrupted cells are then cultured for 1 day on PLL-coated glass-bottom 35-mm dishes or 22-mm coverslips. β -cells are likely to represent 60–80% of the cells in preparations used and can be further selected by identifying by eye the largest cells within the field.
2. *Infection:* 1 day before imaging, cells are infected with adenoviruses at a multiplicity of infection of 30–100 infectious particles per cells for 4 h, and then the culture medium is changed.

3.4. Imaging of Exocytosis

1. Change the culture medium to KRB for 30 min before imaging at 37°C.
2. Transfer the glass-bottom dishes to the thermostat-controlled heating stage (37°C) of the TIRF microscope (system 1).
3. Find fluorescent NPY–Venus-expressing MIN6 cells or infected dispersed primary β -cells.
4. Adjust the laser incident angle to obtain total internal reflection (2).
5. Precisely focus on the cell surface.
6. Lower the laser power or use a neutral density filter to reduce phototoxicity.
7. Increase EM-CCD sensitivity.
8. Acquire images at 30- to 300-ms intervals.
9. Stimulate the cells by changing buffers from KRB to either high glucose- or high-KCl-containing KRB.
10. Continue imaging over 20 min. after changing buffers.

3.5. Labeling Cells for Intracellular Zn^{2+} and Ca^{2+}

1. After overnight culture, disperse islets using Trypsin–EDTA (20–50 islets per well) and plate them on to glass coverslips coated with PLL in 6-well plates.
2. After 24 h in RPMI + 10% FBS, keep cells for 1 h in RPMI containing 3 mM glucose.

3. Load cells with 2 μM Fura Red-AM.
4. For double cation imaging, change media after 25 min to KRB-containing 3 μM fluozin-3 AM and incubate cells for 5 min at 37°C before transferring to a chamber for imaging. At physiological levels of Zn^{2+} there is no significant effect on Fura Red fluorescence (20).

3.6. Imaging of Intracellular Zn^{2+} Concentration

1. Change the culture medium to KRB for 30 min before imaging at 37°C.
2. Transfer the coverslip to a chamber on the stage of the TIRF microscope (system 2) with continuous perfusion with KRB at 37°C.
3. Find a cluster of dispersed primary β -cells loaded with FluoZin-3 (see Note 4).
4. Adjust the laser incident angle to obtain total internal reflection.
5. Precisely focus on the cell surface “footprint.”
6. Lower the laser power or use a neutral density filter to reduce phototoxicity.
7. Acquire images at 30- to 100-ms intervals.
8. Stimulate the cells by changing buffers from KRB to either high glucose- or high-KCl-containing KRB.
9. Continue imaging for 20 min after changing buffers.
10. Obtain the maximum and minimum signal for calibration by changing from KRB to KRB + 5 μM pyrithione or 50 μM TPEN solutions, respectively.

3.7. Imaging of Intracellular Ca^{2+} Concentration (See Note 5)

1. Change the culture medium to KRB for 30 min before the imaging at 37°C.
2. Transfer the coverslip to a chamber on the stage of the TIRF microscope (system 2) with continuous perfusion with KRB at 37°C.
3. Find a cluster of dispersed primary β -cells loaded with Fura Red.
4. Adjust the laser incident angle to obtain a total internal reflection.
5. Precisely focus on the cell surface “footprint.”
6. Lower the laser power or use neutral density filter to reduce phototoxicity.
7. Acquire images at 30- to 100-ms intervals.
8. Stimulate the cells by changing buffers from KRB to either high glucose- or high-KCl-containing KRB. Continue imaging for 20 min.

3.8. Offline Image Analysis

To analyze fusion, single exocytotic events are selected manually, and the average fluorescence intensity of individual vesicle in a $0.7 \times 0.7 \mu\text{m}$ square placed over the vesicle center calculated by using MetaMorph software. To distinguish between fusion events and vesicle movement (i.e., vesicles pause at the plasma membrane and then move back inside the cell without fusing), we monitor the fluorescence changes just before the disappearance of fluorescent signals. When there is a fusion event, a rapid transient increase in fluorescence intensity (to a peak intensity 1.5 times greater than the original fluorescence intensity within 1 s) is observed, whereas when vesicles move, the fluorescence intensity gradually decreases to the background level. The number of fusion events during stimulation period is counted manually based on the above criteria (21). Sequences can be exported as single TIFF files or converted into QuickTime or AVI movies.

3.9. Example of Exocytosis Imaging by TIRF

TIRF microscopy conditions can be used which allow us to observe fluorescence deriving from the fusion of a single vesicle, detect molecules in small numbers and report their function at high temporal and spatial resolution in living cells (Fig. 2a). Induction of a Ca^{2+} influx into the cells by high glucose-containing KRB causes NPY-Venus-containing spots to brighten and spread suddenly, which is consistent with the exocytosis of the fluorescently labeled NPY (Fig. 2b). As shown in Fig. 2b right, the fluorescence increases first in a central region, then spreads into the surrounding area and finally declines as dye diffuses away from the exocytotic site (22). Very rarely, we also observe transient increases in fluorescence that are not associated with the complete disappearance of the fluorescence (Fig. 2c). These events typically exhibit a slower time course (~ 3 s to reach peak fluorescence) than those described above (Fig. 2b, right). Interestingly, much larger vesicle cargoes, such as tissue-type plasminogen activator (tPA), which are found in chromaffin cells (23), show quite different fluorescence intensity changes (Fig. 2d): after an initial increase, tPA-GFP fluorescence describes a much slower time course than the slow disappearance of NPY-Venus (i.e., Fig. 2c) in both PC12 (12) and clonal MIN6 β -cells (24), presumably reflecting either slow release of tPA or vesicle resealing and reacidification (Fig. 2d). In contrast, the slow disappearance of NPY-Venus may reflect the approach of vesicles to the plasma membrane without exocytosis (i.e., vesicle retrieval or vesicle recycling process). In each case TIRF microscopy allows one to track the fate of individual dense-core vesicles before, during, and after exocytosis in living cells.

3.10. Example of Zn^{2+} and Ca^{2+} Imaging by TIRF Imaging

Divalent cations are important signaling molecules in most cell types. Increases in intracellular free (Ca^{2+}) are required for exocytosis (8, 9) and Zn^{2+} release is an important modulator of cell excitability in both neurons (25) and pancreatic α -cells (26).

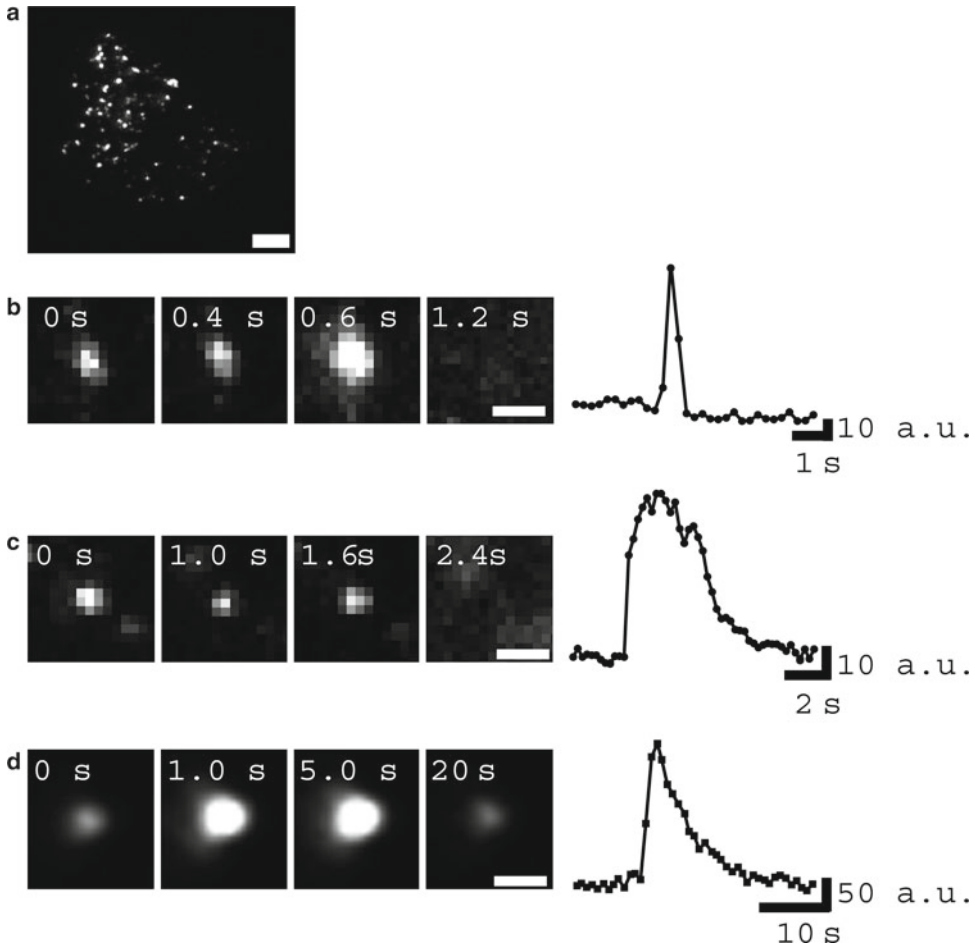


Fig. 2. Effect of high $[K^+]$ stimulation on exocytosis as reported with NPY-Venus-expressing MIN6 cells. **(a)** Typical TIRF image of the cellular distribution of NPY-Venus vesicles in a MIN6 cell. Scale bar: $5\ \mu m$. **(b, left)** Sequential images of a single NPY-Venus expressing vesicle observed after application of high $[K^+]$ stimulation in MIN6 cells. Third image (0.6 s) shows a diffuse cloud of the NPY-Venus fluorescence, and final image (1.2 s) shows an abrupt disappearance of the fluorescent spot. **(b, right, c, right, d, right)** Time course of the fluorescence changes measured in the circles placed in the center of fluorescent spots. The ordinate shows the arbitrary units of brightness. Note that the time scale in **(d)** differs from those in **(b)** and **(c)**. **(c, left)** Sequential images of a single vesicle observed after high $[K^+]$ stimulation without showing any diffuse cloud of the NPY-Venus fluorescence. The third image (1.6 s) does not show any cloud of the dye, while the final image (2.4 s) shows a slow disappearance. **(d, left)** Sequential images of a single vesicle observed after high $[K^+]$ stimulation of the tPA-EGFP fluorescence. Note that tPA-EGFP fluorescence increased initially, and then dimmed slower than those in **(b)** and **(c)**. Scale bars: $1\ \mu m$ (modified from our previous data (21, 22)).

Furthermore, polymorphisms in the *SLC30A8* gene encoding the β -cell specific zinc transporter ZnT8 are associated with type II diabetes and defective insulin granule formation (27). Intracellular free Ca^{2+} has been shown to display both global cytosolic increases and plasma membrane “hot spots” required for normal insulin secretion (28). TIRF microscopy can be used to examine the concentration of Ca^{2+} and Zn^{2+} at the plasma membrane simultaneously

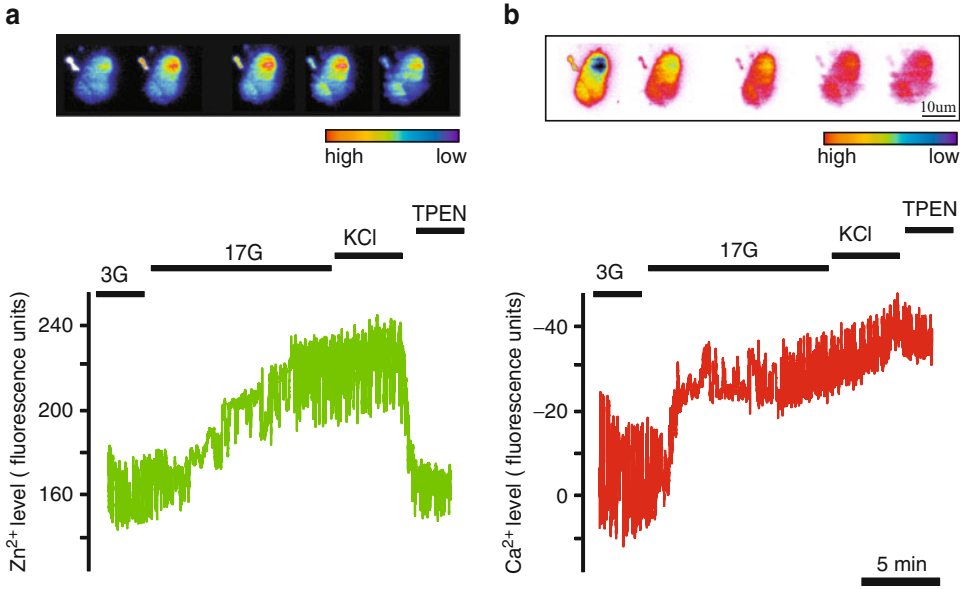


Fig. 3. Effect of glucose and KCl on sub-plasma membrane Zn²⁺ and Ca²⁺ concentrations in primary beta cells. (a, top) Typical representative pseudo-colored images of a primary beta cell at the time points on the trace below. (a, bottom) representative trace of the plasmalemmal Zn²⁺ concentration in response to changes in either glucose (17 mM), KCl, or TPEN. (b, top) Typical pseudo-colored images of a primary beta cell Ca²⁺ at the time points on the trace below. (b, bottom) representative baseline corrected trace of the sub-plasmalemmal Ca²⁺ concentration in response to glucose (17 mM), KCl, or TPEN. Note that the scale is inverted as Fura Red fluorescence at 480 nm excitation decreases in response to increased Ca²⁺ concentration. Scale bar: 10 μm.

in primary beta cells during glucose stimulation (Fig. 3). The cell footprint is defined in the IQ-capture software and the fluorescence intensity measured throughout the time course of the experiment. Figure 3a shows that in response to elevated glucose sub-plasma membrane Zn²⁺ increases, this increase is steady reaching a maximum after about 10 min. The approximate concentration of Zn²⁺ can be calculated from the maximum fluorescence in the presence of 50 μM ZnCl and 5 μM pyrithione and the minimum in the presence of 50 μM TPEN with the K_D of the probe (in the case of FluoZin-3 $K_D = 15$ nM) using the following formula:

$$[Zn^{2+}] = K_D \left(\frac{F_{\min} - F}{F - F_{\max}} \right), \quad (1)$$

where F is the observed fluorescence at a given time. In β-cells the concentration of Zn²⁺ beneath the membrane after glucose stimulation is 1.9 ± 0.18 nM (mean ± S.E.M.). This is at the limit of the sensitivity of the method and equivalent to a two- to threefold increase over the resting cytosolic range of 400–600 pM (29)—well within the expected range for activating a physiological signaling mechanism. Glycinergic receptors, for example, have a zinc

affinity of 27–540 nM (30) and zinc finger proteins, such as those found in many transcription factors, have affinities in the nM–pM range (31). Figure 3b shows the increase in Ca^{2+} in the same cell. The increase in $[\text{Ca}^{2+}]$ occurs at the same time as the increase in $[\text{Zn}^{2+}]$, but appears to reach a maximum value more quickly, although both are sensitive to the L-type calcium channel blocker nifedipine.

4. Conclusion

Here we have described methods for measuring insulin granule movement and sub-plasma membrane divalent cation concentrations using TIRF microscopy. These techniques can be used alongside fluorescently labeled proteins to study the role of each in the control of insulin secretion. By providing near single molecule resolution and dynamic real-time information in single cells these approaches can be combined with the use of healthy, diseased, or genetically modified tissues as a powerful approach to dissecting the regulatory pathways driving exocytosis in both health and disease.

5. Notes

1. During the excitation of fluorescent-labeled vesicles in a single cell (refractive index, $n_2 = 1.38$) adherent to a glass-bottom 35-mm dish (refractive index, $n_1 = 1.53$), wave fronts from a laser light pass through the glass and are reflected from the glass to cell interface at a critical angle α , generating an evanescent wave. The critical angle (α) at which total internal reflection of a laser light hitting the interface between two different refractive indexes substances (i.e., glass and culture medium for TIRF imaging) is determined by:

$$\alpha \geq \sin^{-1} \left(\frac{n_2}{n_1} \right), \quad n_1 > n_2,$$

where n_1 is the refractive index of the glass, n_2 is the refractive index of cells (1.38).

When we use an ultra high NA objective lens (NA = 1.49) to monitor exocytosis, the critical angle for total internal reflection is:

$$\alpha = \sin^{-1} \left(\frac{1.38}{1.53} \right) = 64.41^\circ$$

The maximal achievable angle for total internal reflection by using this objective lens (i.e., n_2 equals NA of objective lens) with glass is:

$$\alpha = \sin^{-1} \left(\frac{1.49}{1.53} \right) = 76.86^\circ$$

Thus, the laser light has to be introduced into the middle of these angles. The decay depth of evanescent field (d) can be calculated theoretically using the formula:

$$d = \frac{\lambda}{4\pi\sqrt{n_1^2 \sin^2 \theta - n_2^2}},$$

where θ is the angle of incidence, λ is the wavelength of the laser. For $\theta = 70^\circ$ and $\lambda = 488$ nm, decay constant (d) becomes 96.3 nm, indicating that a layer of 100–200 nm area from the glass and cell interface is the illumination area of the evanescent wave (32).

2. Other cell types can also be used for imaging; for example, bovine chromaffin cells, PC12 cells, and enteroendocrine cell line GLUtag cells have been tested. The only requirement is that the cells can tightly attach to the glass-bottom 35-mm dishes or coverslips.
3. Imperfect washing of the glass-bottom 35-mm dishes causes the increase of fluorescence background and obstructs the high resolution granule movement and intracellular divalent cations studies.
4. Very high levels of the dye can be toxic. Avoid cells with punctual staining as this can indicate unhealthy cells.
5. Simultaneous measurements of Zn^{2+} and Ca^{2+} are obtained by loading both dyes and using the beam splitter.

References

1. Axelrod D (1981) Cell-substrate contacts illuminated by total internal reflection fluorescence. *J Cell Biol* 89:141–145
2. Axelrod D, Burghardt TP, Thompson NL (1984) Total internal reflection fluorescence. *Annu Rev Biophys Bioeng* 13:247–268
3. Ivarsson R, Jing X, Waselle L, Regazzi R, Renstrom E (2005) Myosin 5a controls insulin granule recruitment during late-phase secretion. *Traffic* 6:1027–1035
4. Kasai K, Ohara-Imaizumi M, Takahashi N et al (2005) Rab27a mediates the tight docking of insulin granules onto the plasma membrane during glucose stimulation. *J Clin Invest* 115:388–396
5. Tomas A, Meda P, Regazzi R, Pessin JE, Halban PA (2008) Munc 18-1 and granuphilin collaborate during insulin granule exocytosis. *Traffic* 9:813–832
6. Wang Z, Thurmond DC (2009) Mechanisms of biphasic insulin-granule exocytosis—roles of the cytoskeleton, small GTPases and SNARE proteins. *J Cell Sci* 122:893–903
7. Cali C, Marchaland J, Regazzi R, Bezzi P (2008) SDF 1- α (CXCL12) triggers glutamate exocytosis from astrocytes on a millisecond

- ond time scale: imaging analysis at the single-vesicle level with TIRF microscopy. *J Neuroimmunol* 198:82–91
8. Becherer U, Moser T, Stuhmer W, Oheim M (2003) Calcium regulates exocytosis at the level of single vesicles. *Nat Neurosci* 6:846–853
 9. Lang T, Wacker I, Steyer J et al (1997) Ca^{2+} -triggered peptide secretion in single cells imaged with green fluorescent protein and evanescent-wave microscopy. *Neuron* 18:857–863
 10. Ohara-Imaizumi M, Nishiwaki C, Kikuta T, Nagai S, Nakamichi Y, Nagamatsu S (2004) TIRF imaging of docking and fusion of single insulin granule motion in primary rat pancreatic beta-cells: different behaviour of granule motion between normal and Goto-Kakizaki diabetic rat beta-cells. *Biochem J* 381:13–18
 11. Steyer JA, Almers W (1999) Tracking single secretory granules in live chromaffin cells by evanescent-field fluorescence microscopy. *Biophys J* 76:2262–2271
 12. Taraska JW, Perrais D, Ohara-Imaizumi M, Nagamatsu S, Almers W (2003) Secretory granules are recaptured largely intact after stimulated exocytosis in cultured endocrine cells. *Proc Natl Acad Sci USA* 100:2070–2075
 13. Tsuboi T, Zhao C, Terakawa S, Rutter GA (2000) Simultaneous evanescent wave imaging of insulin vesicle membrane and cargo during a single exocytotic event. *Curr Biol* 10:1307–1310
 14. Miyazaki J, Araki K, Yamato E et al (1990) Establishment of a pancreatic beta cell line that retains glucose-inducible insulin secretion: special reference to expression of glucose transporter isoforms. *Endocrinology* 127:126–132
 15. Nagai T, Ibata K, Park ES, Kubota M, Mikoshiba K, Miyawaki A (2002) A variant of yellow fluorescent protein with fast and efficient maturation for cell-biological applications. *Nat Biotechnol* 20:87–90
 16. He TC, Zhou S, da Costa LT, Yu J, Kinzler KW, Vogelstein B (1998) A simplified system for generating recombinant adenoviruses. *Proc Natl Acad Sci USA* 95:2509–2514
 17. Diraison F, Motakis E, Parton LE, Nason GP, Leclerc I, Rutter GA (2004) Impact of adenoviral transduction with SREBP1c or AMPK on pancreatic islet gene expression profile: analysis with oligonucleotide microarrays. *Diabetes* 53(Suppl 3):S84–S91
 18. Ainscow EK, Zhao C, Rutter GA (2000) Acute overexpression of lactate dehydrogenase-A perturbs beta-cell mitochondrial metabolism and insulin secretion. *Diabetes* 49:1149–1155
 19. Ravier MA, Rutter GA (2010) Isolation and culture of mouse pancreatic islets for ex vivo imaging studies with trappable or recombinant fluorescent probes. *Methods Mol Biol* 633:171–184
 20. Haugland RP (2009) Hand book of fluorescent probes and research products. Molecular Probes, Eugene
 21. Tsuboi T, Ravier MA, Parton LE, Rutter GA (2006) Sustained exposure to high glucose concentrations modifies glucose signaling and the mechanics of secretory vesicle fusion in primary rat pancreatic beta-cells. *Diabetes* 55:1057–1065
 22. Tsuboi T, Rutter GA (2003) Multiple forms of “kiss-and-run” exocytosis revealed by evanescent wave microscopy. *Curr Biol* 13:563–567
 23. Parmer RJ, Mahata M, Mahata S, Seibald MT, O'Connor DT, Miles LA (1997) Tissue plasminogen activator (t-PA) is targeted to the regulated secretory pathway. Catecholamine storage vesicles as a reservoir for the rapid release of t-PA. *J Biol Chem* 272:1976–1982
 24. Tsuboi T, McMahon HT, Rutter GA (2004) Mechanisms of dense core vesicle recapture following “kiss and run” (“cavapture”) exocytosis in insulin-secreting cells. *J Biol Chem* 279:47115–47124
 25. Bancila V, Nikonenko I, Dunant Y, Bloc A (2004) Zinc inhibits glutamate release via activation of pre-synaptic K channels and reduces ischaemic damage in rat hippocampus. *J Neurochem* 90:1243–1250
 26. Bloc A, Cens T, Cruz H, Dunant Y (2000) Zinc-induced changes in ionic currents of clonal rat pancreatic-cells: activation of ATP-sensitive K^+ channels. *J Physiol* 529(Pt 3):723–734
 27. Nicolson TJ, Bellomo EA, Wijesekara N et al (2009) Insulin storage and glucose homeostasis in mice null for the granule zinc transporter ZnT8 and studies of the type 2 diabetes-associated variants. *Diabetes* 58:2070–2083
 28. Collins SC, Hoppa MB, Walker JN et al (2010) Progression of diet-induced diabetes in C57BL6J mice involves functional dissociation of Ca^{2+} channels from secretory vesicles. *Diabetes* 59:1192–1201
 29. Vinkenborg JL, Nicolson TJ, Bellomo EA, Koay MS, Rutter GA, Merks M (2009) Genetically encoded FRET sensors to monitor intracellular Zn^{2+} homeostasis. *Nat Methods* 6:737–740
 30. Miller PS, Beato M, Harvey RJ, Smart TG (2005) Molecular determinants of glycine receptor alphabeta subunit sensitivities to Zn^{2+} -mediated inhibition. *J Physiol* 566:657–670
 31. Hanas JS, Larabee JL, Hocker JR (2005) Zinc finger interactions with metal and other small molecules. In: Iuchi S, Kuldell N (eds) Zinc Finger proteins: from atomic contact to cellular function. Landes Bioscience, Austin
 32. Ravier MA, Tsuboi T, Rutter GA (2008) Imaging a target of Ca^{2+} signalling: dense core granule exocytosis viewed by total internal reflection fluorescence microscopy. *Methods* 46:233–238

Nanoimaging

Methods and Protocols

Sousa, A.A.; Kruhlak, M.J. (Eds.)

2013, XIV, 510 p. 132 illus., 76 illus. in color., Hardcover

ISBN: 978-1-62703-136-3

A product of Humana Press